Gut Pathogens

RESEARCH

Open Access

Elucidating antibiofilm as well as photocatalytic disinfection potential of green synthesized nanosilver against multi-drug-resistant bacteria and its photodegradation ability of cationic dyes

Bibin Mohan[1†], Padikkamannil Abishad[1†], Pokkittath Radhakrishnan Arya[1], Marita Dias[1], Valil Kunjukunju Vinod[1], Asha Karthikeyan[1], Sanis Juliet[2], Nitin Vasantrao Kurkure[3], Sukhadeo Baliram Barbuddhe[4*], Deepak Bhiwa Rawool[4*] and Jess Vergis[1*]

Abstract

Background Bioinspired nanomaterials have widely been employed as suitable alternatives for controlling biofilm and pathogens due to their distinctive physico-chemical properties.

Methodology This study explored the antibiofilm as well as photocatalytic potential of silver (Ag) nanoparticles (NPs) synthesized using the cell-free supernatant of *Lactobacillus acidophilus* for the disinfection of multi-drug-resistant (MDR) strains of enteroaggregative *E. coli* (EAEC), *Salmonella* Typhimurium, *S.* Enteritidis and methicillin-resistant *Staphylococcus aureus* (MRSA) on exposure to LED light. In addition, the removal of toxic cationic dyes i.e., methylene blue (MB), rhodamine B (RhB) and crystal violet (CV) was explored on exposure to sunlight, LED and UV lights.

Results Initially, the synthesis of AgNPs was verified using UV- Vis spectroscopy, X-ray diffraction and transmission electron microscopy. The synthesized AgNPs exhibited MIC and MBC values of 7.80 and 15.625 µg/mL, respectively. The AgNPs exhibited significant inhibition ($P < 0.001$) in the biofilm-forming ability of all the tested MDR isolates. On exposure to LED light, the AgNPs could effectively eliminate all the tested MDR isolates in a dose-dependent manner. While performing photocatalytic assays, the degradation of RhB was observed to be quite slower than MB and CV irrespective of the tested light sources. Moreover, the sunlight as well as UV light exhibited better photodegradation

†Bibin Mohan and Padikkamannil Abishad contributed equally to this work.

*Correspondence:
Sukhadeo Baliram Barbuddhe
barbuddhesb@gmail.com
Deepak Bhiwa Rawool
deepak.rawool@yahoo.com
Jess Vergis
itzjessvergis@gmail.com

Full list of author information is available at the end of the article

capacity than LED light. Notwithstanding the light sources, RhB followed zero-order kinetics; however, MB and CV followed primarily second-order kinetics.

Conclusion The green synthesized AgNPs were found to be an effective photocatalytic as well as antifouling candidate that could be applied in therapeutics and wastewater treatment.

Keywords Antibiofilm, Disinfection, Dye removal, Nanoparticle, Photocatalysis, Probiotic, Silver

Background

Environmental pollution has become an unsolved dilemma owing to industrialization and population explosion. Water pollution associated with industrial wastes, agricultural runoff, human settlements, and untreated hospital wastes laden with microbes has received global public health attention [1]. The release of industrial dyes and pathogenic bacteria directly to water sources is highly warranted in human and animal settings and causes slight to moderate public health issues [2]. Commonly, dyes such as methylene blue (MB), crystal violet (CV), and rhodamine-B (RhB) which are highly stable and resist biodegradation are frequently employed in industries to produce various polymers, cosmetics, medicines, and food [3]. In general, MB dye is widely used in the medical, biological, and textile industries and is commonly found in agricultural wastewater, whereas RhB is often used in biomedical applications as a stain, coloring agent, photosensitizer, water tracer, and fluorescent marker for microscopic structural study. The CV, commonly used in the textile industry, paints, printing ink, and as a medicinal agent, is discharged in textile industrial effluents. Exposure to water bodies contaminated with these dye-laden industrial effluents can result from slight (tiredness, nausea, skin, and respiratory distress, irritation to the eyes and gastrointestinal tract) to severe (mutagenesis and carcinogenesis) public health issues [4].

Bacterial pathogens such as enteroaggregative *E. coli* (EAEC), non-typhoidal strains of *Salmonella* spp. (*S. enterica* Typhimurium, *S.* Enteritidis), and methicillin-resistant *Staphylococcus aureus* are often derived from livestock farms, human settlements, and hospital wastes [5]. In general, EAEC and *Salmonella* spp. cause mild to moderate diarrhea, abdominal pain, and nausea [6], while MRSA is transmitted through healthcare and community settings causing skin and soft tissue infections, bone and joint infections, and endovascular infections [7]. These pathogenic microbes are often responsible for biofilm-associated infections [5–7]. Of late, the current treatment mechanisms, including biological, chemical, or physical or their combinations are not completely efficient in the removal of these biological and chemical pollutants from water [8]. The bacterial pathogens and industrial dyes could effectively be removed from wastewater by conventional techniques including filtration, ozonation, biodegradation, chlorination, and photocatalysis [9]. However, photocatalysis has received particular attention in recent times, as it breaks down industrial dyes and organic pollutants into smaller components and extremely efficient bacterial killing upon photon absorption [10]. Moreover, photocatalytic disinfection has recently emerged as an eco-friendly technology, due to its high efficiency, strong sterilizing ability, environmentally friendly non-toxic by-product generation, and very mild reaction conditions [11].

Of late, nanomaterials have widely been employed as appropriate alternatives for wastewater treatment due to their high surface area-to-volume ratio, low cost of production, and improved efficiency, along with high surface charge, making them sensible contestants for photocatalytic studies [12]. Green nanotechnology is an emerging field that provides safe nanomaterials with wide biomedical applications and environmental sustainability [13]. Broadly, silver nanoparticles (AgNPs) were investigated for their potential photocatalysis application owing to their oxidation capacity as well as high quantum yield and strongly confined localized surface plasmon resonance [14]. In our earlier study, the antibacterial and anti-fouling properties of antioxidant silver nanoparticles (AgNPs) synthesized using cell-free supernatant of potential probiotic strain against MDR-EAEC were demonstrated [15]. Nonetheless, the AgNPs may compromise the control of pathogenic bacteria harbored in the soil and treatment systems [16, 17], which could be tackled by the photocatalytic disinfection process. However, the photocatalytic properties of the green synthesized AgNPs for bacterial disinfection and dye degradation remain nearly unexplored and constitute an emerging area of interest with environmental implications. In this regard, the present study focuses on exploring the anti-biofilm and photocatalytic potential of AgNPs [15] synthesized using cell-free supernatant of *Lactobacillus acidophilus* (potential probiotic strain) in the killing of MDR isolates of EAEC, NTS, and MRSA on exposure to LED light and for the degradation of MB, CV, and RhB dyes on exposure to different light sources (sunlight, LED, and UV light).

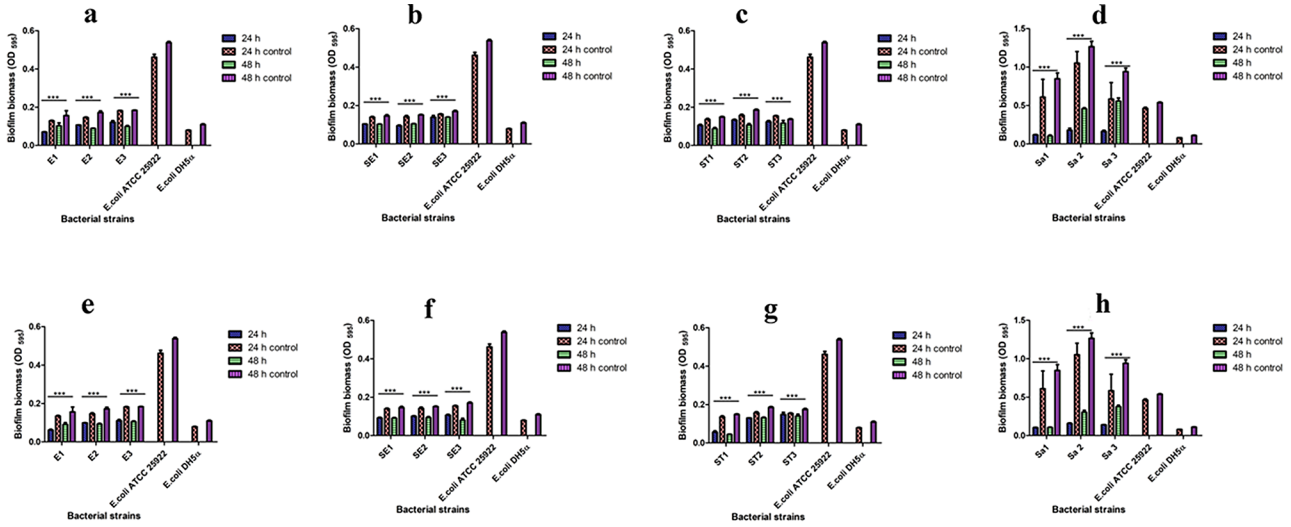

Fig. 1 In vitro antibiofilm potential of AgNPs against MDR bacterial isolates. Images **(a)**, **(b)**, **(c)** and **(d)** denote the antibiofilm potential of AgNPs at MIC (1X) against MDR strains of EAEC (E1, E2, E3), *S.* Enteritidis (S1, S2, S3), *S.* Typhimurium (ST1, ST2, ST3), MRSA (Sa1, Sa2, Sa3) when treated under LED light, while images **(e)**, **(f)**, **(g)**, and **(h)** denote antibiofilm potential of AgNPs at MIC (2X) against MDR strains of EAEC (E1, E2, E3); *S.* Enteritidis (S1, S2, S3), *S.* Typhimurium (ST1, ST2, ST3), MRSA (Sa1, Sa2, Sa3) when treated under LED light, respectively

Methods

Bacterial strains and chemicals

The potential probiotic strain *L. acidophilus* MTCC 10307 for synthesizing AgNPs and the characterized MDR field strains of EAEC (E1; E2; E3), *S.* Enteritidis (S1; S2; S3), *S.* Typhimurium (ST1; ST2; ST3) and MRSA (S1; S2; S3) revalidated using PCR assay [18–20] were maintained in the Department of Veterinary Public Health, College of Veterinary and Animal Sciences, Pookode.

Silver nitrate (≥99% purity; Sigma Aldrich Pvt. Ltd., USA) as well as the cationic dyes (CV, ≥ 88% purity; MB, ≥ 95% purity; and RhB, ≥ 98% purity; Loba Chemie Pvt. Ltd., India) were used in the study. The dehydrated culture media used in this study were procured from HiMedia Laboratories Pvt. Ltd., India.

Synthesis and characterization of AgNPs

The synthesis of AgNPs was performed, as described earlier in our study [21], using a cell-free supernatant of a potential probiotic strain- *L. acidophilus* MTCC 10307. The AgNPs obtained were air-dried, dispersed in nanopure water, and subjected to ultrasonication (Hielscher, Germany) and were verified by UV-Vis spectrophotometer (ThermoFisher Scientific, USA), powder X-ray diffraction (PXRD; Bruker D8 Advance, USA) and transmission electron microscope (TEM; JEM 2100, Jeol, Japan).

In vitro antibacterial activity of AgNPs

The minimum inhibitory concentration (MIC) and minimum bactericidal concentration (MBC) of AgNPs were estimated to assess their in vitro antibacterial activity against MDR strains of EAEC, *S.* Typhimurium, *S.* Enteritidis, and MRSA by co-incubating 50 µL of individual test culture (1×10^7 CFU/mL) in cation-adjusted Mueller Hinton broth (CA-MH; HiMedia) with decreasing concentrations of AgNPs in flat bottom 96-well microtiter plates for 24 h [22]. Subsequently, each well received 0.015% resazurin (HiMedia) dye and was incubated at 37 °C for 30 min to estimate the dye reduction (corresponding to the bacterial inhibition).

The MIC was defined as the lowest concentration of AgNPs at which no discernible growth was observed, while the MBC of the green synthesized AgNPs was determined by plating 10 µL aliquots from each well revealing no visible growth in the corresponding selective agar plates, such as Eosin Methylene Blue (EMB) agar for *E. coli*, Xylose Lysine Deoxycholate (XLD) agar for *S.* Typhimurium and *S.* Enteritidis, and Baird-Parker (BP) agar for MRSA. The MBC of AgNPs was identified as the concentration at which 99.90% of the test cultures were killed.

In vitro antibiofilm-forming activity of AgNPs

Using the CV staining technique in 96-well microtiter plates, the in vitro antibiofilm efficacy of the AgNPs against the tested MDR isolates of EAEC, *S.* Enteritidis, *S.* Typhimurium and MRSA were examined at 24 and 48 h [23].

Briefly, 100 µL of AgNPs (MIC 1X and MIC 2X) were co-incubated with the individual strains of MDR bacteria (10^7 CFU/mL) in sterile nutrient broth (supplemented with 0.45% D-Glucose; HiMedia), with appropriate controls. A single untreated bacterial culture (100 µL) in nutrient broth (100 µL) served as the positive control, while 200 µL of sterile broth served as the negative control. *E. coli* DH5α was utilized as a non-biofilm former in

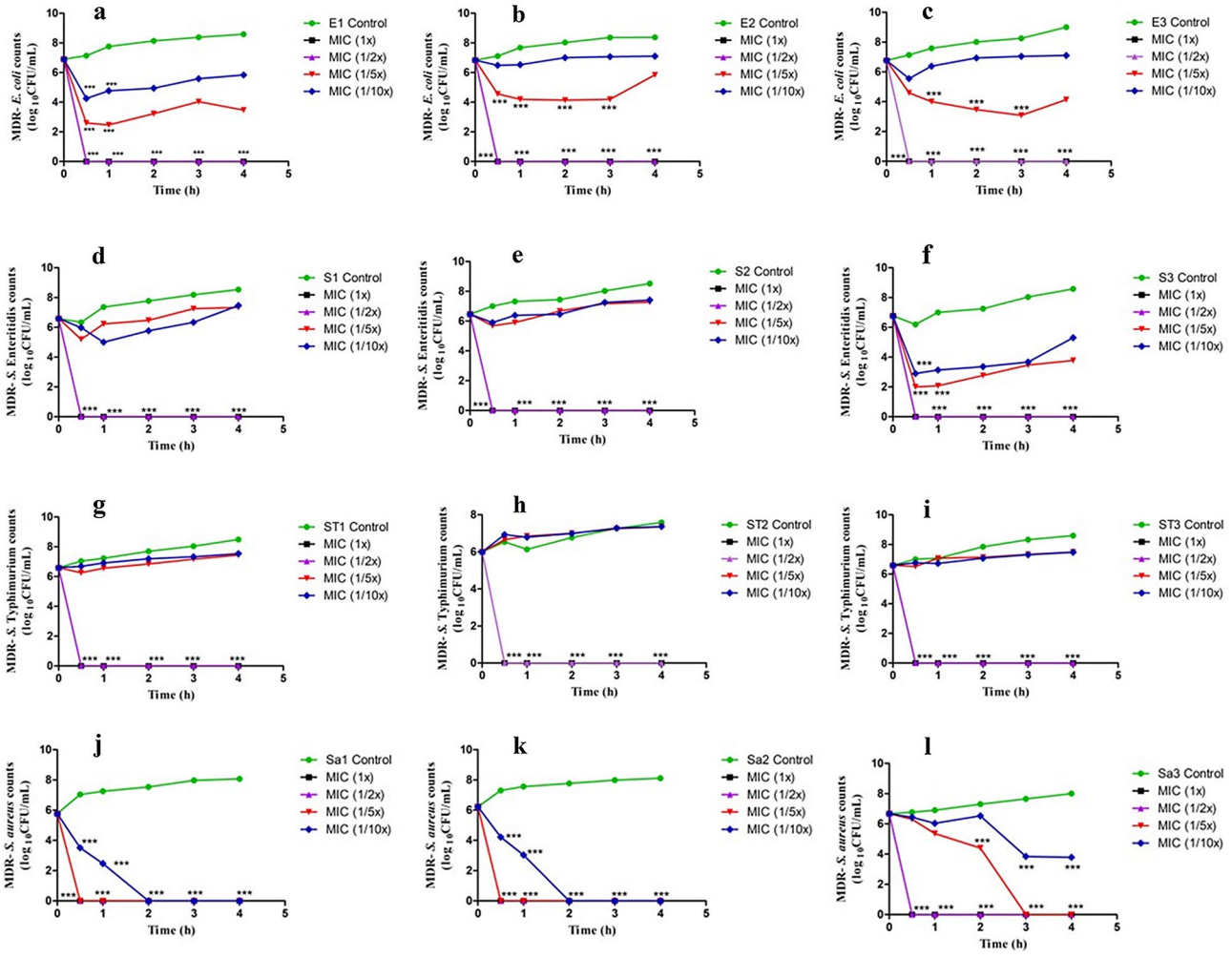

Fig. 2 In vitro dose- and time-dependent photocatalytic disinfection kinetics of MDR bacterial strains treated with AgNPs. Images **(a, b, c)** denote the photocatalytic disinfection kinetics of MDR strains of EAEC (E1, E2, E3), images **(d, e, f)** represent photocatalytic disinfection kinetics of MDR strains of *S.* Enteritidis (S1, S2, S3), images **(g, h, i)** denote photocatalytic disinfection kinetics of MDR strains of *S.* Typhimurium (ST1, ST2, ST3) and images (j, k, l) denote photocatalytic disinfection kinetics of MDR strains of MRSA (Sa1, Sa2, Sa3) when treated with different concentrations of AgNPs (MIC 1X, 1/2X, 1/5X, 1/10X) under LED light

this experiment, while *E. coli* ATCC 25,922 served as a known biofilm-forming strain. Following the incubation at 37 °C, the wells were stained for 30 min with 200 µL of 0.10% CV, and the supernatant which included planktonic cells was removed at 24 and 48 h. Later, the wells were washed thrice with sterile PBS (200 µL), the stain was carefully removed, and 95% ethanol was used to solubilize the stained biofilms that had grown at the bottom of the well.

The absorbance was measured at 595 nm using a Bio-Rad iMark Microplate reader (USA). The reduction in biofilm biomass over 24 h and 48 h was estimated (Eq. 1) as.

$$Biofilm\ reduction\ (\%) = \frac{A_{Control} - A_{Test}}{A_{Control}} \times 100 \quad (1)$$

wherein $A_{Control}$ denotes the absorbance of untreated control taken at 24 h and 48 h, whereas A_{Test} denotes the absorbance of treated samples taken at 24 h and 48 h.

In vitro dose- and time-dependent photocatalytic disinfection of MDR bacterial strains treated with AgNPs

An in vitro dose- and time-dependent extracellular growth kinetics [23] was used to assess the photocatalytic antibacterial efficacy of green synthesized AgNPs against the MDR test strains of EAEC, *S.* Typhimurium, *S.* Enteritidis, and MRSA on exposure to LED light. The log-phase bacterial cultures (1×10^7 CFU/mL) in CA-MH broth were incubated with four different doses of green synthesized AgNPs (1X MIC, 1/2X MIC, 1/5X MIC, and 1/10X MIC) to assess the photocatalytic in vitro growth kinetics of MDR isolates of EAEC ($n=3$), *S.* Typhimurium ($n=3$), *S.* Enteritidis ($n=3$) and MRSA

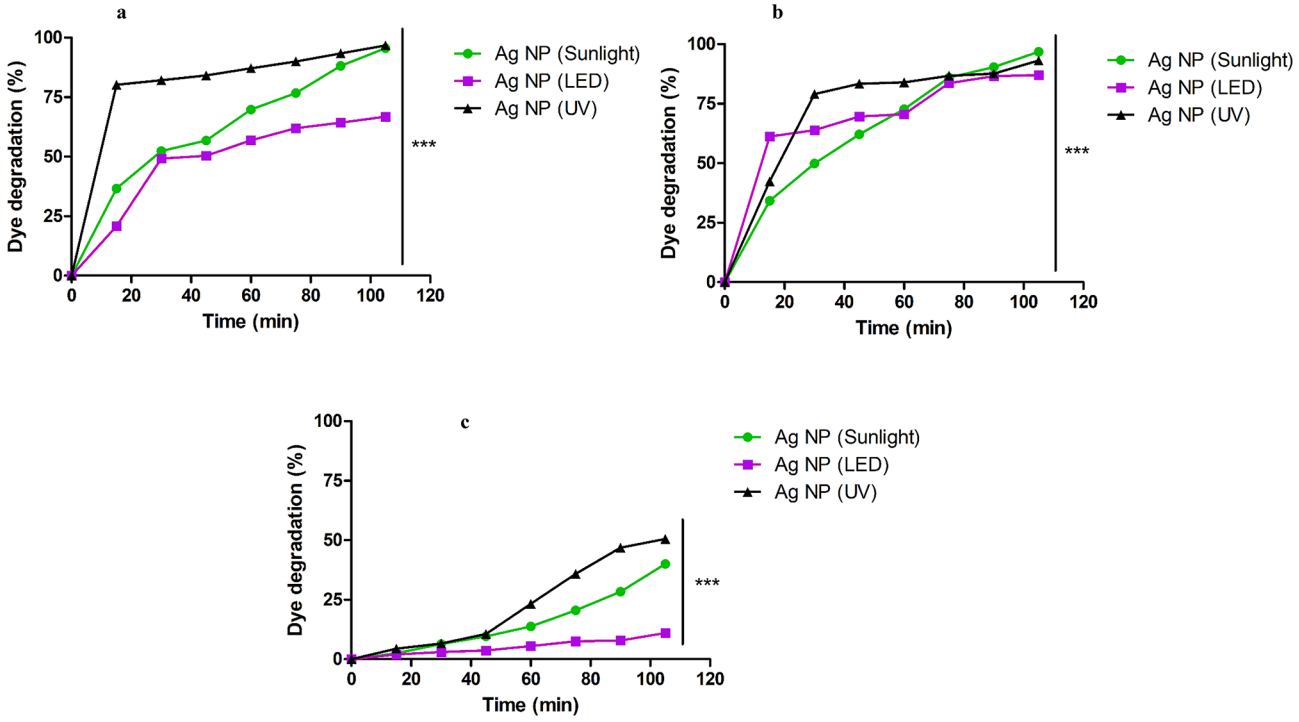

Fig. 3 Degradation pattern of cationic dyes when treated with AgNPs on exposure to various light sources. Images **(a, b, c)** denote degradation of MB, CV and RhB, respectively on exposure to sunlight, UV and LED light when treated with AgNPs (0.50 mg/mL)

(n=3). An untreated control consisting of the respective test isolates in CA-MH broth was utilized as control. The light source was kept at a distance of 15 cm from the treatment groups in order to obtain the desired lux.

To measure the growth of MDR test isolates, aliquots (10 µL) from all the groups were drawn at 0, 30, 60, 120, 180, and 240 min, serially diluted and plated on EMB agar plates for MDR-EAEC, XLD agar plates for MDR-NTS and BP agar plates for MDR-MRSA [24]. After the incubation period at 37 °C for 18 to 24 h, the individual colonies were counted, and were expressed as $\log_{10}$ CFU/mL.

Table 1 Reduction in biofilm biomass of MDR isolates when exposed to MIC (1X and 2X) of probiosynthesized AgNPs measured over 24 and 48 h

MDR bacterial strains	Strains	Biofilm reduction (%)			
		MIC (1X)		MIC (2X)	
		24 h	48 h	24 h	48 h
EAEC	E1	39.837	64.563	46.875	64.563
	E2	29.801	42.949	36.943	42.949
	E3	41.899	46.409	43.429	54.128
S. Enteritidis	S1	21.212	47.399	27.273	50.521
	S2	27.692	34.899	32.168	49.246
	S3	34.416	41.270	35.714	49.112
S. Typhimurium	ST1	30.496	48.993	52.482	69.231
	ST2	41.488	41.667	22.024	26.882
	ST3	33.553	37.640	33.721	38.579
MRSA	Sa1	85.417	85.594	87.240	89.720
	Sa2	80.548	82.993	86.033	88.163
	Sa3	75.163	80.064	81.664	84.130

Photocatalytic dye degradation ability of AgNPs

The synthesized AgNPs were treated with MB, CV, and RhB dyes (Loba Chemie, India) on exposure to different light sources viz., sunlight, LED, and UV light [25]. The initial concentration of the photocatalyst and dyes were optimized. Briefly, the aqueous solution of individual dyes (5 ppm for MB and RhB, and 50 ppm for CV) was mixed with individual NPs (final concentration of 0.50 mg/mL); untreated dyes served as a control. The dye-NP mixtures were then agitated in a magnetic stirrer (Neuation Technologies Pvt. Ltd, India) and kept at 300 rpm for 15 min in the dark to obtain an adsorption-resorption isotherm. Later, the mixtures were exposed separately to sunlight (11.5408348°, 76.0209177°; 52100 lx), LED light (63400 lx, 460 nm, 50 W [Opple, India]), and UV light (260 nm, 16 W [Violight, India]). The LED and UV light were kept at a distance of 15 cm from the sample to obtain the desired lux. The reactions were performed at ambient conditions (pH 7.0; room temperature 25 °C).

The samples drawn at specific intervals (0, 15, 30, 45, 60, 75, 90, and 105 min) were then centrifuged for 15 min at 5000 rpm. The absorbance was recorded at 670, 592, and 550 nm for MB, CV, and RhB, respectively [12, 26] using a UV-Vis spectrophotometer (ThermoFisher

Scientific Pvt. Ltd., USA). Further, the concentration of the dyes was estimated from their absorbance using Beer-Lemberts law [27]. The degradation of dye in solution (%) was estimated [28, 29; Eq. 2] by

$$\boldsymbol{Degradation}\ (\%) = \frac{\boldsymbol{C_0 - C_1}}{\boldsymbol{C_0}} \times\ 100 = \frac{\boldsymbol{A_0 - A_1}}{\boldsymbol{A_0}} \times\ 100 \quad (2)$$

where C_0 denotes the concentration of the control, C_1 is the concentration of the sample at a specific time point, A_0 is the amplitude of the control at its peak absorbance wavelength, and A_1 is the peak absorbance of the dye at a specific time point. The photodegradation of the dyes was estimated as a function of exposure time over AgNPs.

Determination of degradation kinetics

To quantify the photocatalytic reaction, different orders of kinetics were analyzed viz., zero-order (Eq. 3), first-order (Eq. 4), pseudo-first-order (Eq. 5), and second order (Eq. 6), with its rate constants:

$$\boldsymbol{C_1} = -\boldsymbol{kt} + \boldsymbol{C_o} \quad (3)$$

$$\boldsymbol{lnC_1} = -\boldsymbol{kt} + \boldsymbol{lnC_0} \quad (4)$$

$$\boldsymbol{ln}\frac{\boldsymbol{C_1}}{\boldsymbol{C_0}} = -\boldsymbol{kt} \quad (5)$$

$$\frac{1}{\boldsymbol{C_1}} = \boldsymbol{kt} + \frac{1}{\boldsymbol{C_0}} \quad (6)$$

where the rate constant is *k* is expressed as $molL^{-1}min^{-1}$ for zero-order, min^{-1} for first order, and pseudo-first-order and $Lmol^{-1}min^{-1}$ for second-order reactions [29, 30].

Statistical analysis

Each experiment was performed three times in triplicate and the results were analyzed using GraphPad Prism 8.2.1 (GraphPad Software Inc., San Diego, CA, USA). The photocatalytic i*n vitro* dose- and time-dependent extracellular growth kinetics of the tested MDR isolates and the photocatalytic dye degradation experiments were analyzed using a two-way (repeated measurements) ANOVA with a Bonferroni multiple comparison post-test. P-values ≤ 0.05 were regarded as statistically significant, while $P \leq 0.01$ was highly significant.

Results and discussion

Synthesis and characterization of AgNPs

The decline phase cell-free extract of potential probiotic *L. acidophilus* strain and aqueous solution of silver nitrate (0.10 M) in the ratio of 1:4 was used for the green synthesis of AgNPs. The formation of the AgNPs was visualized by the change in the color of the solution to brownish white from an initial colorless solution. Earlier, the green synthesis of AgNPs was achieved using a variety of botanicals [31–38] bacteria [39], fungi [40], seaweeds [41] and cyanobacterium [42] for wide biological and clinical applications.

UV-Vis spectroscopy was performed to detect the surface plasmon resonance of the AgNPs [43] which exhibited a characteristic peak at 430 nm (Supplementary Fig. 1a). In addition, PXRD analysis carried out for the confirmation of crystallinity, presence, size and phase variety of the AgNPs revealed diffraction peaks (2θ) at 27.7°, 32.1°, 33.4°, 46.1°, 54.6°, 57.3°, and 76.4° (Supplementary Fig. 1b). It is possible to attribute the peaks to the planes (98), (101), (200), and (311), which show face-centered cubic structure in nano silver structure correlated with the JCPDS card: number 00–004-0783 [44]. Further, the average size of the AgNPs was estimated by using Debye–Scherrer's equation and was found to be 46 nm. The morphological study conducted using TEM imaging revealed spherical-shaped monodisperse AgNPs with sizes extending from 10 to 20 nm (Supplementary Fig. 1c). This could be attributed to the capping of organic molecules during the synthesis [45]. SAED pattern exhibited concentric rings (Supplementary Fig. 1d) suggestive of crystallinity [46].

In vitro antibacterial activity

For all the tested MDR isolates (EAEC, *S.* Typhimurium, *S.* Enteritidis, and MRSA), the MIC values were determined to be 7.80 µg/mL, while the MBC values were determined to be 15.625 µg/mL. The comparatively lower MIC values of AgNPs against all the tested bacterial strains could be attributed to the mode of synthesis, the presence of functional groups from the bioactive molecules used in the synthesis, the surface nature of the NPs, ionic strength, and the pH of the resulting nanoparticle [47]. The ability of AgNPs to generate reactive oxygen species (ROS) forms an integral part of their antibacterial ability [48].

In vitro antibiofilm activity

In general, biofilms provide bacteria with a sheltered antibiotic-resistant environment [49]. In order to infiltrate host cells and facilitate the development of infection, pathogenic bacteria use the creation of biofilm communities as a crucial tactic [50]. The biofilms originated over the industries pose a major public health threat. The condition would be aggravated when the biofilms are recovered in the food and medical industry resulting in food-borne illnesses as well as healthcare-associated threats. Consequently, it is imperative to explore diverse approaches to mitigate bacterial adhesion and biofilm formation [51].

Given their ability as a potential antibacterial agent, AgNPs could be utilized for treating bacterial biofilms. By using the CV staining technique, we examined whether green synthesized AgNPs could inhibit the ability of the MDR isolates to form biofilms both at 24 and 48 h. The AgNPs (1X MIC and 2X MIC) were found to inhibit the biofilm-forming ability of the tested MDR strains in a highly significant ($P<0.001$) manner after 24 h, since all the tested isolates exhibited a reduction in the biofilm biomass when compared to their respective controls (untreated bacterial cultures) (Fig. 1). Furthermore, during a 48 h period, all the MDR isolates treated with the AgNPs exhibited a significant ($P<0.001$) reduction in their ability to form biofilms (Fig. 1). It was also observed that in comparison to 24 h, the AgNPs inhibited the ability of the MDR test isolates to form biofilms more at 48 h (Table 1). An overall reduction in the biofilm biomass was observed to be higher in MDR-MRSA strains as compared to the MDR strains of EAEC and *Salmonella* spp. (Table 1). This difference in biomass reduction (Table 1) could be due to the changes in the composition of the cell wall of Gram-positive (MRSA) when compared to the Gram-negative (EAEC and *Salmonella* spp.) bacteria [52]. It was reported that the AgNPs work against bacterial biofilms either by disruption in the intermolecular force or attachment of bacterial cells with the surfaces. Besides, AgNPs have been able to block quorum sensing [53]. Since the MDR isolates were susceptible to AgNPs, it could be considered an excellent candidate to prevent and inhibit the formation of biofilm produced by bacterial pathogens.

In vitro dose- and time-dependent photocatalytic killing kinetics of MDR bacterial strains treated with AgNPs

The time-kill kinetic assay of individual MDR-EAEC, *S.* Typhimurium, *S.* Enteritidis, and MRSA strains co-cultured with the four different concentrations (1X MIC, 1/2X MIC, 1/5X MIC, and 1/10X MIC) of green synthesized AgNPs along with their respective controls on exposure to LED light was estimated (Fig. 2). Sunlight and UV light were not used in these experiments because they have proven bactericidal activity [54, 55].

In this study, all the MDR isolates (EAEC, *S.* Typhimurium, *S.* Enteritidis, and MRSA), exhibited a progressively increasing growth pattern at 30, 60, 120, 180, and 240 min of incubation (Fig. 2). The MDR strains of EAEC, *S.* Typhimurium and *S.* Enteritidis isolates did not exhibit discernible growth after 30 min of incubation ($P<0.001$) when treated with AgNPs at 1X MIC and 1/2X MIC (Fig. 2a and i). Interestingly, two strains of MDR-MRSA (Sa1 and Sa2) when treated with MIC and well as sub-MIC levels (1X MIC, 1/2X MIC, and 1/5X MIC) did not exhibit visible growth patterns after 30 min of incubation. Moreover, when treated with 1/10X MIC of AgNPs, no growth could be visualized in the MDR-MRSA strains (Sa1 and Sa2) after 120 min of co-incubation ($P<0.001$) (Fig. 2j and k). Nevertheless, the Sa3 strain when co-incubated with AgNPs (1X MIC and 1/2X MIC) exhibited no visible bacterial growth after 30 min and 180 min with 1/5X MIC. No elimination of the Sa3 strain of MDR-MRSA could be observed when treated with 1/10X MIC of AgNPs (Fig. 2l). The photoexcitation abilities of AgNPs which in turn resulted in an enhanced ROS production could be effectively utilized for their photocatalytic disinfection as well as dye degradation abilities [56].

Earlier researchers have reported ≥95% photo-inactivation potential of *S. epidermis* and *S. aureus* [57, 58]. In our earlier study, the time taken for complete bacterial elimination was observed to be 240 min for the non-photocatalytic time-dependent antibacterial activity of AgNPs [21] at their MIC doses. This enhanced antibacterial activity of the AgNPs observed in the present

Table 2 Determination of photocatalytic dye degradation potential and order of reaction on treatment AgNPs under different light sources

	Sunlight			LED light			UV light		
	MB	CV	RhB	MB	CV	RhB	MB	CV	RhB
Time (min)	**Degradation (%)**								
15	34.24	36.59	2.53	61.24	20.83	2.03	42.36	80.19	4.45
30	49.87	52.41	6.38	63.88	49.18	3.01	79.02	82.12	6.63
45	62.10	56.83	9.61	69.63	50.40	3.73	83.40	84.13	10.66
60	72.68	69.78	13.83	70.52	56.90	5.54	83.97	87.14	23.30
75	85.99	76.68	20.58	83.63	61.95	7.51	86.74	89.94	35.85
90	90.37	88.16	28.35	86.50	64.30	7.88	87.59	93.40	46.89
105	96.80	95.53	40.06	87.03	66.80	11.04	93.20	96.49	49.11
Kinetics									
Order	Second	First	Zero	Second	Second	Zero	Second	Second	Zero
R^2value	0.944	0.932	0.937	0.922	0.902	0.974	0.913	0.909	0.924
Intercept	0.001	-0.026	-0.004	0.059	0.008	-0.001	0.073	0.082	-0.006
Slope	0.939	0.086	1.268	0.823	0.626	1.139	1.675	0.394	1.208

photocatalytic experiment could be due to the higher quantum of ROS generated, which actively participates in bacterial killing, upon photoexcitation from a light source. Nonetheless, the complete elimination of MDR-MRSA as well as EAEC strains could be due to the extracellular nature of the bacterial pathogens when compared to the *Salmonella* strains which are capable of dwelling in distinct niches with varying rates of replication [59]. The photocatalytic disinfection studies of the AgNPs revealed the fact that bacterial elimination could be achieved in a dose- and time-dependent manner.

Photocatalytic dye degradation abilities of AgNPs

The green synthesized AgNPs exhibited a drastic increase (20–80%) in the photodegradation pattern for MB and CV dyes (Fig. 3) from the initial timepoint, regardless of the light source. Nonetheless, the degradation of RhB when treated with AgNPs was gradual throughout the entire duration. Surprisingly, on exposure to LED, degradation of RhB was found to be minimal (11%) (Table 2; Fig. 3c). Nonetheless, the dye degradation activity of the AgNPs in dark was non-significant as compared to that of photocatalytic dye degradation experiments. Sunlight was chosen as one of the light sources, because it is naturally available in a wide area with a diverse spectrum of colors, and wavelengths in nearly equal amounts, whereas UV light was chosen for its short frequency and high energy photon production. The LEDs were selected because of their low energy usage, availability, and extended shelf life.

Sunlight consists of approximately 45% visible spectra and 5% UV irradiation [60]. Furthermore, UV light was considered as it consists of high-frequency, non-ionizing radiations with short wavelengths ranging from 100 to 300 nm, thus producing high-energy photons owing to its high photoexcitation abilities on photocatalyst surfaces [61]. Moreover, AgNPs exert their photocatalytic properties owing to the ability of surface plasmon resonance (SPR) which maximizes at 450 nm [62]. The stability of RhB towards degradation could be attributed to its high stability and solubility in water [63]. The proposed mechanisms for photocatalytic degradation of the dyes include dye sensitization by charge induction, dye degradation by indirect oxidation/reduction, and direct dye photolysis [64].

Determination of degradation kinetics

According to the reaction parameters obtained, RhB fitted in zero-order kinetics, whereas MB followed second-order kinetics in all the cases irrespective of the light source (Table 2). Similarly, CV followed second-order kinetics throughout the experiment except on exposure to sunlight, wherein first-order kinetics was exhibited (Table 2). A zero-order reaction is a chemical reaction in which the rate remains constant when the reactant concentration increases or decreases, whereas a chemical reaction that has a reaction rate that is linearly dependent on the concentration of just one component is referred to as a first-order reaction [65]. Moreover, a reaction that depends on the square of one reactant's concentration or the product of two reactant concentrations is considered second-order [66]. Nonetheless, a bimolecular or second-order reaction that is made to behave like a first-order reaction is known as a pseudo-first-order reaction. This reaction takes place when one responding material is present in significant excess or is kept at a steady concentration concerning the other substance [67], The difference in the reaction order of the dye degradation by AgNPs upon exposure to different light sources could be associated with the generation of hot-charge carriers, elevated temperatures, and focused electromagnetic fields upon absorption and scattering of light from different sources of light [68].

It is well known that electrons from the filled valence band (VB) are promoted to the conduction band (CB) when AgNPs are photo-induced by irradiation from light sources with photonic energy (hv) either equal to or greater than the excitation energy (Eg), which would produce electron-hole (e/h+) pairs. The electron-hole pairs formed migrate to the surface of NPs and participate in redox processes, in which H^+ ions combine with water and hydroxide ions (OH^-) to form hydroxyl radicals ($OH^\bullet$), and the electrons react with oxygen to produce anionic superoxide radicals ($O_2^{\bullet-}$) and hydrogen peroxide (H_2O_2). The subsequent reaction between H_2O_2 and $O_2^{\bullet-}$ will produce $OH^\bullet$, which is a strong oxidizing agent [69–71]. These ROS generated will attack the dyes adsorbed (MB, RhB, and CV) on the surface of the AgNPs to produce intermediate compounds, which would ultimately result in the formation of relatively non-toxic molecules such as CO_2, H_2O, and mineral acids [72]. Similarly, the ROS will attack the bacterial cell wall which would result in bacterial killing and reduction in biofilm biomass formation. Besides, the pH of the solution plays an important role in determining the photodegradation capacity. It was documented that a better photocatalytic ability exhibited in the basic solution than acidic could due to the dominating surface reaction and was favored in alkaline conditions [73, 74], which needs more investigation.

In addition, a molecular mechanism of dye degradation has also been postulated wherein the functional genes related to the electron transport, oxidoreductase activity, and superoxide metabolism of organic matter were upregulated which could accelerate in photodegradation potential of nanoparticles [75]. Several key genes including glutathione S-transferase enrichment were reported to be involved in degrading azo dyes and electron transport, and undecaprenyl-diphosphatase, carbon storage

regulator, and DNA ligase enrichment were associated in response to dyes and photocatalysts [75]. The functional role of such genes along with the electronic mechanism would contribute to a better understanding of photodegradation of cationic dyes in wastewater.

Conclusion

In short, this study evaluated the antibiofilm as well as photocatalytic disinfection capabilities of green synthesized AgNPs on exposure to LED light against MDR strains of EAEC, *S.* Typhimurium, *S.* Enteritidis and MRSA along with photocatalytic dye degradation potential against MB, CV, and RhB on exposure to sunlight, LED and UV lights. The MIC value obtained for the AgNPs was determined to be 7.80 µg/mL against all the tested MDR isolates of EAEC, NTS, and MRSA. The AgNPs exhibited significant antibiofilm potential both at 1X and 2X MIC levels. The photocatalytic disinfection assays demonstrated that the time required for bacterial elimination at MIC levels was relatively lower than in the non-photocatalytic experiments. In addition, the dye degradation experiments exhibited that on exposure to different light sources, the AgNPs could degrade MB, CV, and RhB. Notwithstanding the light sources, RhB followed zero-order kinetics; however, MB and CV followed primarily second-order kinetics. However, the degradation of RhB was quite slower than MB and CV irrespective of different light sources. The sunlight as well as UV light exhibited better photodegradation capacity than LED light. Further, the photocatalytic potential of AgNPs could be enhanced by doping or conjugating them with other nanomaterials. This would potentiate their scientific utility in the field of therapeutics and wastewater treatment mediated by way of potential photocatalytic, antimicrobial, and antibiofilm ability.

Supplementary Information

The online version contains supplementary material available at https://doi.org/10.1186/s13099-024-00639-3.

Supplementary Material 1

Acknowledgements

The authors thank the Vice-Chancellor and Director of Academics and Research of KVASU, Dean, CVAS, Pookode, and the Director of ICAR- National Meat Research Institute, Hyderabad for providing the necessary facilities for the research. The authors are grateful to Dr. Sandeep K., Government Victoria College, Kerala for proofreading the manuscript.

Author contributions

Conceptualisation [SBB, DBR, JV]; Fund acquisition [SBB, DBR, JV, NVK]; Resources [SBB, DBR, JV]; Software [BM, PA]; Data Curation [PRA, MD, VVK, AK, SJ]; Methodology [BM, PA, PRA, MD, VVK]; Investigation [BM, PA]; Validation [PRA, MD]; Visualisation [BM, PA, VVK, AK, SJ]; Supervision [SBB, DBR, JV]; Writing the original draft [BM, PA, PRA, MD, VVK]; Editing and final drafting [SBB, NVK, DBR, JV]. All authors read and approved the final version of the manuscript.

Funding

This work was supported by a grant from the ICAR-National Agricultural Science Fund (ICAR-NASF; NASF/ABA-8007) to SBB, DBR, JV, and NVK. This work was supported by the M.V.Sc. student research support (KVASU/DAR/Acad/A3/30315/2023) from KVASU, Pookode to BM and JV.

Data availability

No datasets were generated or analysed during the current study.

Declarations

Ethics approval and consent to participate

Not applicable.

Consent for publication

All authors have given consent for publication.

Competing interests

S.B. Barbuddhe is an Associate Editor for Gut Pathogens. The authors declare no other competing interests.

Author details

[1]Department of Veterinary Public Health, College of Veterinary and Animal Sciences, Kerala Veterinary and Animal Sciences University, Pookode, Wayanad 673 576, India
[2]Department of Veterinary Pharmacology and Toxicology, College of Veterinary and Animal Sciences, Kerala Veterinary and Animal Sciences University, Pookode, Wayanad 673 576, India
[3]Department of Veterinary Pathology, Nagpur Veterinary College, Nagpur 440 006, India
[4]ICAR- National Meat Research Institute, Hyderabad 500 092, India

Received: 17 July 2024 / Accepted: 27 August 2024
Published online: 27 September 2024

References

1. Xu H, Jia Y, Sun Z, Su J, Liu QS, Zhou Q, Jiang G. Environmental pollution, a hidden culprit for health issues. Eco-Environment Health. 2022;1(1):31–45. https://doi.org/10.1016/j.eehl.2022.04.003.
2. Islam T, Repon MR, Islam T, Sarwar Z, Rahman MM. Impact of textile dyes on health and ecosystem: a review of structure, causes, and potential solutions. Environ Sci Pollut Res. 2023;30(4):9207–42. https://doi.org/10.1007/s11356-022-24398-3.
3. Al-Buriahi AK, Al-Gheethi AA, Kumar PS, Mohamed RM, Yusof H, Alshalif AF, Khalifa NA. Elimination of rhodamine B from textile wastewater using nanoparticle photocatalysts: a review for sustainable approaches. Chemosphere. 2022;287:132162. https://doi.org/10.1016/j.chemosphere.2021.132162.
4. Hemashenpagam N, Selvajeyanthi S. Textile dyes and their effect on human beings. InNanohybrid materials for treatment of textiles dyes 2023 Sep 21 (pp. 41–60). Singapore: Springer Nature Singapore. https://doi.org/10.1007/978-981-99-3901-5_3
5. Huda N, Nahar GN, Hossain T, Rahman A, Rus'd AA, Ahmed T. Growth and prevalence of antibiotic-resistant Bacteria in Waste from Pagla Treatment Plant. https://doi.org/10.20944/preprints202307.0935.v1
6. Abishad P, Niveditha P, Unni V, Vergis J, Kurkure NV, Chaudhari S, Rawool DB, Barbuddhe SB. In silico molecular docking and in vitro antimicrobial efficacy of phytochemicals against multi-drug-resistant enteroaggregative Escherichia coli and non-typhoidal Salmonella spp. Gut Pathog. 2021;13:1–1. https://doi.org/10.1186/s13099-021-00443-3.
7. Tigabu A, Getaneh AL. Staphylococcus aureus, ESKAPE Bacteria Challenging Current Health Care and Community settings: a literature review. Clin Lab. 2021 Aug;1(7). 10.7754/. Clin.Lab.2020.200930.
8. Donkadokula NY, Kola AK, Naz I, Saroj D. A review on advanced physico-chemical and biological textile dye wastewater treatment techniques. Rev Environ Sci Biotechnol. 2020;19:543–60. https://doi.org/10.1007/s11157-020-09543-z.

9. Mecha AC, Chollom MN. Photocatalytic ozonation of wastewater: a review. Environ Chem Lett. 2020;18(5):1491–507. https://doi.org/10.1007/s10311-020-01020-x.
10. Nagajyothi PC, Veeranjaneya Reddy L, Devarayapalli KC, Prabhakar Vattikuti SV, Wee YJ, Shim J. Environmentally friendly synthesis: photocatalytic dye degradation and bacteria inactivation using Ag/f-MWCNTs composite. J Clust Sci. 2021;32:711–8. https://doi.org/10.1007/s10876-020-01821-8.
11. Sabariselvan L, Okla MK, Brindha B, Kokilavani S, Abdel-Maksoud MA, El-Tayeb MA, Al-Ghamdi AA, Alatar AA, Sivaranjani PR, Khan SS. Interfacial coupling of CuFe2O4 induced hotspots over self-assembled g-C3N4 nanosheets as an efficient photocatalytic bacterial disinfectant. Environ Pollut. 2024;342:123076.
12. Saravan RS, Muthukumaran M, Mubashera SM, Abinaya M, Prasath PV, Parthiban R, Mohammad F, Oh WC, Sagadevan S. Evaluation of the photocatalytic efficiency of cobalt oxide nanoparticles towards the degradation of crystal violet and methylene violet dyes. Optik. 2020;207:164428. https://doi.org/10.1016/j.ijleo.2020.164428.
13. Samuel MS, Ravikumar M, John JA, Selvarajan E, Patel H, Chander PS, Soundarya J, Vuppala S, Balaji R, Chandrasekar N. A review on green synthesis of nanoparticles and their diverse biomedical and environmental applications. Catalysts. 2022;12(5):459. https://doi.org/10.3390/catal12050459.
14. Brindha B, Okla MK, Kokilavani S, Sabariselvan L, Al-amri SS, Abdel-Maksoud MA, Harini G, Alshuwaish R, Alsakkaf WA, Khan SS. Dynamic Ag-mediated electron transfer confined ZnO nanorods for boosted photocatalytic bacterial disinfection. J Clean Prod. 2024;451:141908.
15. Prasastha V, Yasur J, Abishad P, Ramesh C, Purushottam D, Radhakrishnan P et al. Journal of Drug Delivery Science and Technology Enhanced therapeutic efficacy of biogenic nanosilver-conjugated thymol: *In vitro* and *in vivo* evaluation against emerging multi-drug resistant microbes. J Drug Deliv Sci Technol. 2023;86:104741. https://doi.org/10.1016/j.jddst.2023.104741
16. Khan S, Mukherjee A, Chandrasekaran N. Silver nanoparticles tolerant bacteria from sewage environment. J Environ Sci. 2011;23(2):346–52.
17. Sudheer Khan S, Bharath Kumar E, Mukherjee A, Chandrasekaran N. Bacterial tolerance to silver nanoparticles (SNPs): Aeromonas punctata isolated from sewage environment. J Basic Microbiol. 2011;51(2):183–90.
18. Nair A, Rawool DB, Doijad S, Poharkar K, Mohan V, Barbuddhe SB, Kolhe R, Kurkure NV, Kumar A, Malik SV, Balasaravanan T. Biofilm formation and genetic diversity of Salmonella isolates recovered from clinical, food, poultry and environmental sources. Infect Genet Evol. 2015;36:424–33. https://doi.org/10.1016/j.meegid.2015.08.012.
19. Vijay D, Dhaka P, Vergis J, Negi M, Mohan V, Kumar M, Doijad S, Poharkar K, Kumar A, Malik SS, Barbuddhe SB. Characterization and biofilm forming ability of diarrhoeagenic enteroaggregative Escherichia coli isolates recovered from human infants and young animals. Comp Immunol Microbiol Infect Dis. 2015;38:21–31. https://doi.org/10.1016/j.cimid.2014.11.004.
20. Sahebnasagh R, Saderi H, Owlia P. The prevalence of resistance to Methicillin in Staphylococcus aureus strains isolated from patients by PCR method for Detec-tion of mecA and Nuc genes. Iran J Public Health. 2014;43(1):84.
21. Abishad P, Vergis J, Unni V, Ram VP, Niveditha P, Yasur J, Juliet S, John L, Byrappa K, Nambiar P, Kurkure NV. Green synthesized silver nanoparticles using Lactobacillus acidophilus as an antioxidant, antimicrobial, and antibiofilm agent against multi-drug resistant enteroaggregative Escherichia coli. Probiotics Antimicrob. 2022;14(5):904–14. https://doi.org/10.1007/s12602-022-09961-1.
22. Wayne PA. Clinical and laboratory standards institute. Performance standards for antimicrobial susceptibility testing.
23. Vergis J, Malik SS, Pathak R, Kumar M, Ramanjaneya S, Kurkure NV, Barbuddhe SB, Rawool DB. Antimicrobial efficacy of indolicidin against multi-drug resistant enteroaggregative Escherichia coli in a Galleria mellonella model. Front Microbiol. 2019;10:2723. https://doi.org/10.3389/fmicb.2019.02723.
24. Miles AA, Misra SS, Irwin JO. The estimation of the bactericidal power of the blood. J Hyg (Lond). 1938;38:732–49.
25. Abishad P, Jayashankar M, Namratha K, Nayan MB, Kurkure NV, Barbuddhe SB, Rawool DB, Vergis J, Byrappa K. Zeolite imidazole framework (Fe) nanostructure: a simple and efficient dye degradation catalyst under visible light. Inorg Chem Commun. 2023;147:110058. https://doi.org/10.1016/j.inoche.2022.110058.
26. Waghchaure RH, Adole VA, Jagdale BS. Photocatalytic degradation of methylene blue, rhodamine B, methyl orange and eriochrome black T dyes by modified ZnO nanocatalysts: a concise review. Inorg Chem Commu. 2022;143:109764. https://doi.org/10.1016/j.inoche.2022.109764.
27. Aslam Z, Rahman RS, Shoab M, Khan ZM, Zulfequar M. Photocatalytic response of CuCdS2 nanoparticles under solar irradiation against degradation of Methylene Blue dye. Chem Phys Lett. 2022;804:139883. https://doi.org/10.1016/j.cplett.2022.139883.
28. Muthuvel A, Jothibas M, Manoharan C. Synthesis of copper oxide nanoparticles by chemical and biogenic methods: photocatalytic degradation and in vitro antioxidant activity. Nanotechnol Environ Eng. 2020;5(2):14. https://doi.org/10.1007/s41204-020-00078-w.
29. Lanjwani MF, Khuhawar MY, Khuhawar TM, Lanjwani AH, Memon SQ, Soomro WA, Rind IK. Photocatalytic degradation of eriochrome black T dye by ZnO nanoparticles using multivariate factorial, kinetics and isotherm models. J Clust Sci. 2023;34(2):1121–32. https://doi.org/10.1007/s10876-022-02293-8.
30. Song WC, Kim B, Park SY, Park G, Oh JW. Biosynthesis of silver and gold nanoparticles using Sargassum Horneri extract as catalyst for industrial dye degradation. Arab J Chem. 2022;15(9):104056. https://doi.org/10.1016/j.arabjc.2022.104056.
31. Kim DY, Saratale RG, Shinde S, Syed A, Ameen F, Ghodake G. Green synthesis of silver nanoparticles using Laminaria Japonica extract: characterization and seedling growth assessment. J Clean Prod. 2018;172:2910–8.
32. Sathishkumar P, Preethi J, Vijayan R, Yusoff AR, Ameen F, Suresh S, Balaguruna-than R, Palvannan T. Anti-acne, anti-dandruff and anti-breast cancer efficacy of green synthesised silver nanoparticles using Coriandrum sativum leaf extract. J Photochem Photobiol B. 2016;163:69–76.
33. Ameen F, Srinivasan P, Selvankumar T, Kamala-Kannan S, Al Nadhari S, Almansob A, Dawoud T, Govarthanan M. Phytosynthesis of silver nanoparticles using Mangifera indica flower extract as bioreductant and their broad-spectrum antibacterial activity. Bioorg Chem. 2019;88:102970.
34. Mohanta YK, Panda SK, Syed A, Ameen F, Bastia AK, Mohanta TK. Bio-inspired synthesis of silver nanoparticles from leaf extracts of Cleistanthus collinus (Roxb.): its potential antibacterial and anticancer activities. IET Nanobiotechnol. 2018;12(3):343–8.
35. Almansob A, Bahkali AH, Albarrag A, Alshomrani M, Binjomah A, Hailan WA, Ameen F. Effective treatment of resistant opportunistic fungi associated with immuno-compromised individuals using silver biosynthesized nanoparticles. Appl Nanosci. 2022;12(12):3871–82.
36. Deepa AF, Amirul Islam M, Dhanker R. Green synthesis of silver nanoparticles from vegetable waste of pea Pisum sativum and bottle gourd Lagenaria siceraria: characterization and antibacterial properties. Front Environ Sci. 2022;10:941554.
37. Ramar K, Gnanamoorthy G, Mukundan D, Vasanthakumari R, Narayanan V, Jafar Ahamed A. Environmental and antimicrobial properties of silver nanoparticles synthesized using Azadirachta indica juss leaves extract. SN Appl Sci. 2019;1:1–1.
38. Gomathi A, Kuppusamy MR, Aruna K, Sridhar TM. Preparation of metal doped nanoparticles using flower extract of Piper betle and its anti-bacterial investigations. Materials Today: Proceedings. 2023 Feb 20.
39. Ameen F, AlYahya S, Govarthanan M, ALjahdali N, Al-Enazi N, Alsamhary K, Alshehri WA, Alwakeel SS, Alharbi SA. Soil bacteria Cupriavidus sp. mediates the extracellular synthesis of antibacterial silver nanoparticles. J Mol Struct. 2020;1202:127233.
40. Ameen F, Al-Homaidan AA, Al-Sabri A, Almansob A, AlNAdhari S. Anti-oxidant, anti-fungal and cytotoxic effects of silver nanoparticles synthesized using marine fungus Cladosporium halotolerans. Appl Nanosci. 2023;13(1):623–31.
41. Valarmathi N, Ameen F, Almansob A, Kumar P, Arunprakash S, Govarthanan M. Utilization of marine seaweed Spyridia filamentosa for silver nanoparticles synthesis and its clinical applications. Mater Lett. 2020;263:127244.
42. Ameen F, Abdullah MM, Al-Homaidan AA, Al-Lohedan HA, Al-Ghanayem AA, Almansob A. Fabrication of silver nanoparticles employing the cyanobacterium Spirulina platensis and its bactericidal effect against opportunistic nosocomial pathogens of the respiratory tract. J Mol Struct. 2020;1217:128392.
43. Singh D, Bansal A, Jain A, Tyagi LK, Mondal S, Patel RK. GC-MS based lemon grass metabolite analysis involved in the synthesis of silver nanoparticles and evaluation of photo-catalytic degradation of methylene blue. Biometals. 2021;34(5):1121–39. https://doi.org/10.1007/s10534-021-00337-6.
44. El-Moslamy SH, Elkady MF, Rezk AH, Abdel-Fattah YR. Applying Taguchi design and large-scale strategy for mycosynthesis of nano-silver from endophytic Trichoderma Harzianum SYA. F4 and its application against phytopathogens. Sci Rep. 2017;7(1):45297. https://doi.org/10.1038/srep45297.
45. Rauwel P, Küünal S, Ferdov S, Rauwel E. A review on the green synthesis of silver nanoparticles and their morphologies studied via TEM. Adv Mater Sci Eng. 2015;2015(1):682749. https://doi.org/10.1155/2015/682749.

46. Singh T, Jyoti K, Patnaik A, Singh A, Chauhan R, Chandel SS. Biosynthesis, characterization and antibacterial activity of silver nanoparticles using an endophytic fungal supernatant of Raphanus sativus. J Genetic Eng Biotechnol. 2017;15(1):31–9. https://doi.org/10.1016/j.jgeb.2017.04.005.
47. Lakkim V, Reddy MC, Pallavali RR, Reddy KR, Reddy CV, Inamuddin, Bilgrami AL, Lomada D. Green synthesis of silver nanoparticles and evaluation of their antibacterial activity against multidrug-resistant bacteria and wound healing efficacy using a murine model. Antibiotics. 2020;9(12):902. https://doi.org/10.3390/antibiotics9120902.
48. Lee W, Kim KJ, Lee DG. A novel mechanism for the antibacterial effect of silver nanoparticles on *Escherichia coli*. Biometals. 2014;27:1191–201. https://doi.org/10.1007/s10534-014-9782-z.
49. Alfei S. Shifting from ammonium to Phosphonium salts: a Promising Strategy to develop Next-Generation weapons against Biofilms. Pharmaceutics. 2024;16(1):80. https://doi.org/10.3390/pharmaceutics16010080.
50. Kaur T, Putatunda C, Vyas A, Kumar G. Zinc oxide nanoparticles inhibit bacterial biofilm formation via altering cell membrane permeability. Prep Biochem Biotechnol. 2021;51(4):309–19. https://doi.org/10.1080/10826068.2020.1815057.
51. Khelissa SO, Abdallah M, Jama C, Faille C, Chihib NE. Bacterial contamination and biofilm formation on abiotic surfaces and strategies to overcome their persistence. J Mater Environ Sci. 2017;8(9):3326–46.
52. Sharma R, Lalhall A, Puri S, Wangoo N. Design of Fmoc-Phenylalanine Nanofibrillar Hydrogel and mechanistic studies of its Antimicrobial Action against both gram-positive and Gram-negative Bacteria. ACS Appl Bio Mater. 2023;6(2):494–506. https://doi.org/10.1021/acsabm.2c00767.
53. Swidan NS, Hashem YA, Elkhatib WF, Yassien MA. Antibiofilm activity of green synthesized silver nanoparticles against biofilm associated enterococcal urinary pathogens. Sci Rep. 2022;12(1):3869. https://doi.org/10.1038/s41598-022-07831-y.
54. Azuma T, Hayashi T. Effects of natural sunlight on antimicrobial-resistant bacteria (AMRB) and antimicrobial-susceptible bacteria (AMSB) in wastewater and river water. Sci Total Environ. 2021;766:142568. https://doi.org/10.1016/j.scitotenv.2020.142568.
55. Rezaie A, Leite GG, Melmed GY, Mathur R, Villanueva-Millan MJ, Parodi G, Sin J, Germano JF, Morales W, Weitsman S, Kim SY. Ultraviolet a light effectively reduces bacteria and viruses including coronavirus. PLoS ONE. 2020;15(7):e0236199. https://doi.org/10.1371/journal.pone.0237782.
56. Sahoo B, Rath SK, Champati BB, Panigrahi LL, Pradhan AK, Nayak S, Kar BR, Jha S, Arakha M. Photocatalytic activity of biosynthesized silver nanoparticle fosters oxidative stress at nanoparticle interface resulting in antimicrobial and cytotoxic activities. Environ Toxicol. 2023;38(7):1577–88. https://doi.org/10.1002/tox.23787.
57. Swetha S, Abdel-Maksoud MA, Okla MK, Janani B, Dawoud TM, El-Tayeb MA, Khan SS. Triple-mechanism driven Fe-doped nn hetero-architecture of Pr6O11-MoO3 decorated g-C3N4 for doxycycline degradation and bacterial photoinactivation. Chem Eng J. 2023;461:141806.
58. Swedha M, Okla MK, Abdel-Maksoud MA, Balasurya S, Al-Amri SS, Alaraidh IA, Alatar AA, Alsakkaf WA, Khan SS. Construction of Ag/CdZnS QDs nanocomposite for enhanced visible light photoinactivation of Staphylococcus aureus. Environ Pollut. 2024;348:123749.
59. Luk CH, Enninga J, Valenzuela C. Fit to dwell in many places–the growing diversity of intracellular Salmonella niches. Front Cell Infect Microbiol. 2022;12:989451. https://doi.org/10.3389/fcimb.2022.989451.
60. Arora I, Chawla H, Chandra A, Sagadevan S, Garg S. Advances in the strategies for enhancing the photocatalytic activity of TiO2: Conversion from UV-light active to visible-light active photocatalyst. Inorg Chem Commun. 2022;143:109700. https://doi.org/10.1016/j.inoche.2022.109700.
61. Serpone NA, Emeline AV. Semiconductor Photocatalysis Past, Present, and Future Outlook. J Phys Chem Lett. 2012;3(5):673–7. https://doi.org/10.1021/jz300071j.
62. Adrianto N, Panre AM, Istiqomah NI, Riswan M, Apriliani F, Suharyadi E. Localized surface plasmon resonance properties of green synthesized silver nanoparticles. Nano-Struct Nano-Objects. 2022;31:100895. https://doi.org/10.1016/j.nanoso.2022.100895.
63. Mzimela N, Tichapondwa S, Chirwa E. Visible-light-activated photocatalytic degradation of rhodamine B using WO 3 nanoparticles. RSC Adv. 2022;12(53):34652–9. https://doi.org/10.1039/D2RA06124D.
64. Saeed M, Muneer M, Haq AU, Akram N, Photocatalysis. An effective tool for photodegradation of dyes—A review. Environ Sci Pollut Res. 2022;29(1):293–311. https://doi.org/10.1007/s11356-021-16389-7.
65. Kumar KV, Porkodi K, Rocha AF. Langmuir–Hinshelwood kinetics–a theoretical study. Catal Commun. 2008;9(1):82–. https://doi.org/10.1016/j.catcom.2007.05.019. 4.
66. Ho YS. Review of second-order models for adsorption systems. J Hazard Mater. 2006;136(3):681–9. https://doi.org/10.1016/j.jhazmat.2005.12.043.
67. Corbett JF. Pseudo first-order kinetics. J Chem Educ. 1972;49(10):663. https://doi.org/10.1021/ed049p663.
68. Kumari G, Kamarudheen R, Zoethout E, Baldi A. Photocatalytic surface restructuring in individual silver nanoparticles. ACS Catal. 2021;11(6):3478–86. https://doi.org/10.1021/acscatal.1c00478.
69. Swetha S, Alahmadi TA, Ansari MJ, Khan SS. Strategically tailored double S-scheme heterojunction in h-MoO3 doped Bi7O9I3 decorated with Cr–CdS quantum dots for efficient photocatalytic degradation of phenolics. J Clean Prod. 2024;449:141656.
70. Dutta V, Sonu S, Raizada P, Thakur VK, Ahamad T, Thakur S, Kumar Verma P, Quang HH, Nguyen VH, Singh P. Prism-like integrated Bi2WO6 with Ag-CuBi2O4 on carbon nanotubes (CNTs) as an efficient and robust S-scheme interfacial charge transfer photocatalyst for the removal of organic pollutants from wastewater. Environ Sci Pollut Res. 2023;30(60):124530–45.
71. Senthilmurugan B, Okla MK, Abdel-Maksoud MA, Al-Amri SS, Alaraidh IA, Alatar AA, Hassan AH, Sheteiwy MS, AbdElgawad H, Khan SS. Interface engineered Ag-r-GO-CuFe2O4-Fe3O4 heterojunction an efficient photocatalyst for water treatment and toxicity study in Trifolium plants. J Ind Eng Chem. 2024;135:344–55.
72. Kanniah P, Radhamani J, Chelliah P, Muthusamy N, Joshua Jebasingh Sathiya Balasingh Thangapandi E, Reeta Thangapandi J, Balakrishnan S, Shanmugam R. Green synthesis of multifaceted silver nanoparticles using the flower extract of *Aerva lanata* and evaluation of its biological and environmental applications. ChemistrySelect. 2020;5(7):2322–31. https://doi.org/10.1002/slct.201903228.
73. Guo Y, Zhou C, Fang L, Liu Z, Li W, Yang M. Effect of pH on the catalytic degradation of rhodamine B by synthesized CDs/g-C3N4/Cu x O composites. ACS Omega. 2021;6(12):8119–30.
74. Nguyen Thi Thu T, Nguyen Thi N, Tran Quang V, Nguyen Hong K, Nguyen Minh T. Le Thi Hoai N. Synthesis, characterisation, and effect of pH on degradation of dyes of copper-doped TiO2. J Exp Nanosci. 2016;11(3):226–38.
75. Chen J, Liu K, Liu Y. Synergistic molecular mechanism of degradation in dye wastewater by Rhodopseudomonas palustris intimately coupled carbon nanotube-silver modified titanium dioxide photocatalytic composite with sodium alginate. J Environ Manage. 2024;351:119913.

Publisher's note